Appl. Phys. B (2016) 122:124
DOI 10.1007/s00340-016-6398-8

Applied Physics B
Lasers and Optics

Multi-octave supercontinuum generation with IR radiation filamentation in transparent solid-state media

S. A. Frolov[1] · V. I. Trunov[1] · V. E. Leshchenko[1] · E. V. Pestryakov[1]

Received: 21 January 2015 / Accepted: 24 March 2016 / Published online: 27 April 2016

Abstract Supercontinuum generation from the near to far IR during radiation filamentation in solid-state media in an anomalous dispersion region is theoretically investigated. The initial search for appropriate media with the use of an interference model showed that the widest IR spectrum is generated in media with high values of zero group velocity dispersion wavelength with the pump wavelength located not far from it. Halides belong to one of such media groups. The possibility of generation of a very wide supercontinuum in calcium fluoride (0.52–3.35 μm, which corresponds to 2.7 octaves), sodium chloride (0.7–7.6 μm, 3.5 octaves), and potassium iodide (0.66–22 μm, 5.1 octaves) is demonstrated by numerical simulation. Also, pulse self-compression down to 13 fs at the 5-μm central wavelength (about single period) has been observed in potassium iodide. The mechanisms of multi-octave supercontinuum generation are discussed.

1 Introduction

In recent years, coherent sources of ultrabroadband femtosecond radiation have been widely used for diagnostic purposes [1–3]. There exist two conventional methods for generation of such supercontinuum (SC): fiber propagation and filamentation. The former method usually allows to achieve wider spectra than the one with filamentation [4, 5] due to a longer propagation distance in the fiber. The main disadvantage of this method is low energy values of generated SC, which reach tens or hundreds of nJ. On the other hand, filamentation allows to reach energy of tens of μJ in bulk media and tens of mJ in gases. One of the parameters important for spectroscopy is reproducibility of the generated spectra, which is usually low in the case of fiber propagation due to pulse splitting and spectra modulation [6] and high for bulk media filamentation [7] with certain conditions.

Since the problem of spectrum broadening (especially in the far-IR region) and generation efficiency increase is very important, we believe that filamentation is most promising for obtaining more energy in the SC. IR-range filamentation in bulk media has another advantage which is anomalous dispersion in this spectral region. It is important that anomalous dispersion causes pulse self-steepening which, in turn, leads to relatively strong generation of short wavelengths. This makes it possible to generate both several-octave wide spectra [7] and self-compressed pulses [7–9]. More theoretical research of peculiarities of filamentation in anomalous dispersion region can be found in [10–14]. It should be noted that generation of multi-octave wide SC as well as pulse compression in gases has also been demonstrated both theoretically [15–17] and experimentally [18].

Recently we conducted research on influence of band gap on width of generated SC in solid-state media [19] where potassium bromide demonstrated possibility of generation of a very wide SC. In this paper, we move forward and investigate the media for a very wide IR supercontinuum generation. For the initial assessment of the SC width, we used the so-called interference model [20] more extensively, which allowed us to perform preliminary estimation of the generated spectra width. These results are discussed in Sect. 2; to confirm them after the initial analysis, we perform direct simulation of the filamentation. The model and code used for the simulation are presented in Sect. 3, and its results are analyzed in Sect. 4.

✉ S. A. Frolov
stanislav.a.frolov@gmail.com

[1] Institute of Laser Physics, Siberian Branch of the Russian Academy of Sciences, Prosp. Akad. Lavrentyeva 13/3, Novosibirsk, Russia 630090

2 Interference model

The width of the SC generated during filamentation greatly depends on the medium and pump radiation parameters. The phenomenological three-wave mixing model allows us to find regions of frequency–angular spectra where the SC is generated most effectively [7]. Further development of this approach, also called an interference model [20], makes it possible to estimate the qualitative shape of the generated frequency–angular spectra if only the medium dispersion is known. As a result, we have a method for search of the optimum medium and pump wavelength for SC generation. Below we consider only the case of mid- to far-IR pump wavelengths, which are the most promising for obtaining the widest SC extending from the visible to far IR. To find the most promising medium, we analyzed a large number of optical glasses and crystals which are transparent in IR region.

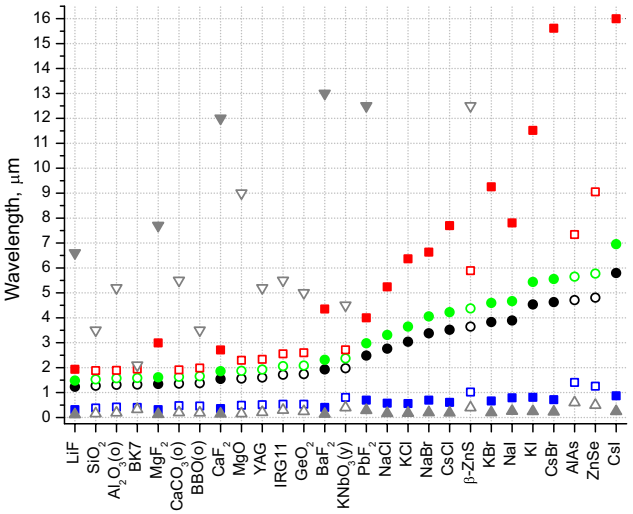

Fig. 1 SC borders (short-wavelength border is shown by *blue squares*, and long-wavelength one by *red squares*) computed with the interference model for a pump wavelength of 1.2 $\lambda_{GVD=0}$ (*green circles*) for a number of media. Also shown are the zero GVD wavelength (*black circles*) and the transparency range (*gray triangles*); *filled symbols* stand for halides and *hollow ones*, for other media

It has been found that for the given group of media (halides or oxides) there is a qualitative similarity of the frequency–angular spectra for a given ratio of the pump wavelength λ_p to the zero group velocity dispersion (GVD) wavelength $\lambda_{GVD=0}$. The SC borders calculated with the interference model in the case of $\lambda_p/\lambda_{GVD=0} = 1.2$ in a number of media are presented in Fig. 1. These borders were obtained by the integrating the results of interference model over angle (expression (9) from [20] multiplied by λ^3 to compensate for wavelength-dependent tilt of spectra as shown in Fig. 2) and correspond to 10^{-1} level. The following trend is clear: The higher the value of zero GVD wavelength $\lambda_{GVD=0}$, the further the SC long-wavelength border moves to IR (especially for halides), whereas the short-wavelength border tends to increase much more slowly. Although in case of halides $\lambda_{GVD=0}$ and long-wavelength transparency boundary are slightly correlated, there

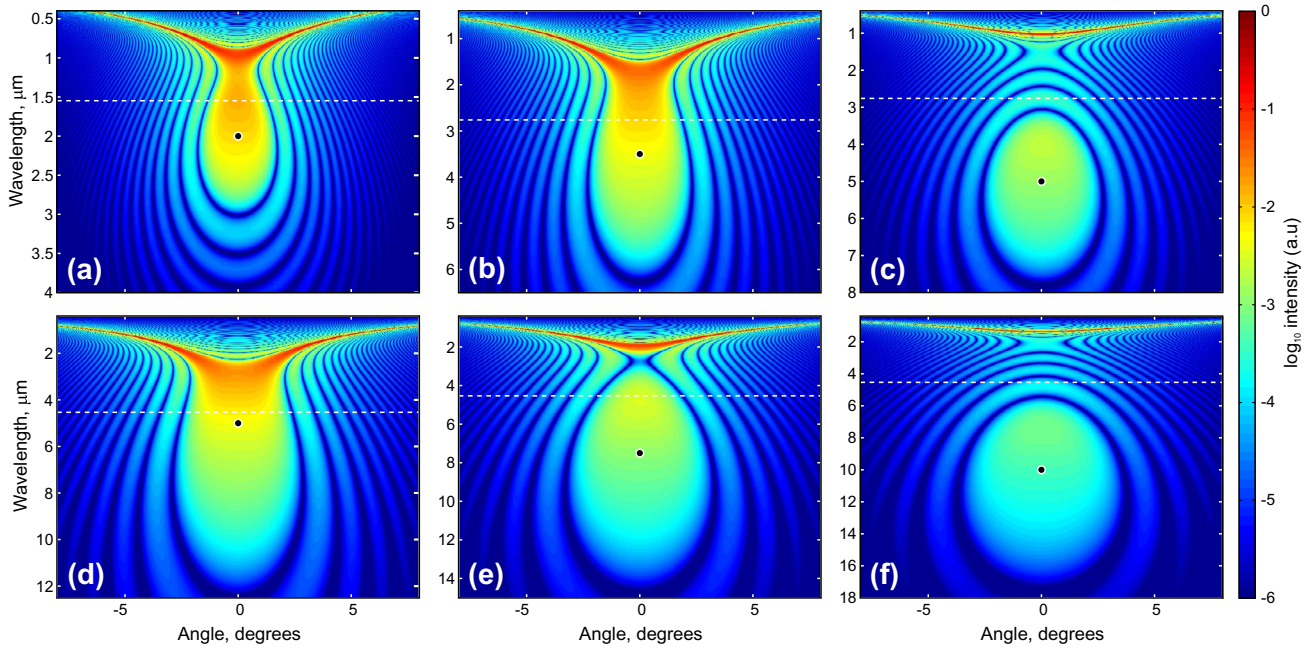

Fig. 2 Frequency–angular spectra of SC calculated with the interference model. **a** CaF_2, 2 μm pump, **b** NaCl, 3.5 μm pump, **c** NaCl, 5 μm pump, **d** KI, 5 μm pump, **e** KI, 7.5 μm pump, **f** KI, 10 μm pump

is no such correlation for long-wavelength SC boundary as it is observed with $\lambda_{GVD=0}$. Thus, we propose that the zero GVD wavelength is reasonably good indicator for IR SC width, which considerably simplifies the search for media for SC generation in mid to far-IR region.

The common group of optical media characterized with the longest $\lambda_{GVD=0}$ and the widest obtained SC includes halides, in particular, iodides, for instance, for potassium iodide $\lambda_{GVD=0} = 4.5$ μm and for cesium iodide, $\lambda_{GVD=0} = 5.3$ μm. Thus, for our further investigation we took the following commonly used optical media: calcium fluoride (CaF_2), sodium chloride (NaCl), and potassium iodide (KI). These media were chosen owing to their wide use and, hence, the possibility of carrying out future experiments, and also because they have known properties that are important for simulation. The calculated interference model spectra are presented in Fig. 2, and the SC parameters in Table 1. Dispersive relations used for calculation are presented in Table 2.

One of the most important known limitations of the interference model is a constant frequency–angular spectrum of the emitting source, which greatly limits the predictive properties of the model [20]. In fact, the source spectrum is nonconstant both over the propagation distance and in the frequency–angular domain due to various properties of the medium and pump radiation. Therefore, we performed a simulation of filamentation for the above-mentioned media.

Table 1 SC width calculated with the interference model

Medium	Pump wavelength (μm)	Potential SC range (μm)	SC width (octaves)
CaF_2	2	0.5–3	2.6
NaCl	3.5	0.75–6	3
NaCl	5	0.7–7.6	3.4
KI	5	0.9–11.5	3.7
KI	7.5	0.9–13.6	3.9
KI	10	0.93–15	4

3 Filamentation model

We used the forward Maxwell equation (FME) equation to describe the spatiotemporal evolution of a laser pulse envelope during filamentation in transparent media [21]:

$$\frac{\partial \widehat{A}}{\partial z} = \frac{i}{2k(\omega)}\nabla_{\perp}^2\widehat{A} + i[k(\omega)-\kappa(\omega)]\widehat{A} + i\frac{\omega}{c}\frac{n(\omega_0)}{n(\omega)}n_2\widehat{|A|^2A} - \frac{U_i}{2}\frac{\widehat{W_{PI}}}{|A|^2}A - \frac{\sigma(\omega)}{2}(1+i\omega\tau_c)\widehat{\rho A}, \quad (1)$$

where A is the electric field, $\widehat{B}$ is the Fourier transform of B, $k(\omega) = n(\omega)\omega/c$ is the pump wave vector, $n(\omega)$ is the refractive index (see Table 2 for dispersive relation references), $\kappa(\omega) = k(\omega_0) - (\omega-\omega_0)/v_g$, ω_0 is the central pulse frequency, v_g is the group velocity at frequency ω_0, n_2 is the nonlinear part of the refractive index, $\sigma(\omega) = \frac{q_e^2}{\varepsilon_0 n(\omega) c m_e}\frac{\tau_c}{1+\omega^2\tau_c^2}$ is the inverse bremsstrahlung cross section, τ_c is the characteristic electron collision time, q_e and m_e are the electron charge and mass, respectively, ε_0 is the dielectric constant, ρ is the plasma density, U_i is the band gap, W_{PI} is the photoionization rate defined by the Keldysh formalism (except for the above-mentioned parameters, it depends on the reduced effective electron–hole mass m^*) [22]. Note that frequency term in front of nonlinear refractive index also accounts for pulse self-steepening. The plasma evolution is described by the following equation [21]:

$$\frac{\partial \rho}{\partial t} = W_{PI}(|A|) + \frac{\sigma(\omega_0)}{U_i}\rho|A|^2, \quad (2)$$

which includes photoionization and avalanche ionization as plasma sources.

Equations (1–2) take into account the following effects: the Kerr effect self-focusing, plasma defocusing, photo- and avalanche ionization, as well as the full medium dispersion. This allows us to simulate pulses of up to few wave periods. Also unlike amorphous media such as fused silica halides do not exhibit noticeable Raman response

Table 2 Medium's parameters used in the simulation

Parameter	CaF_2	NaCl	KI
n_2 (10^{-16} cm^2/W)	1.92 [26]	4.35 [27]	29 [28]
U_i (eV)	10 [29]	9 [29]	6.2 [29]
m^* (m_e)	0.6 [30]	0.6 [30]	0.21 [30]
τ_c (fs)	3	3	3
$\lambda_{GVD=0}$ (μm)	1.55	2.76	4.53
P_{cr} (MW)	22 @ 2 μm	27.9 @ 3.5 μm, 57.1 @ 5 μm	8 @ 5 μm, 18 @ 7.5 μm
Transparency region (μm)	0.12–10	0.17–18	0.25–39
Reference to dispersion relation	[31]	[32]	[32]
Crystal length (mm)	6	5	4

[23] which is two orders of magnitude lower than that of fused silica, so we omit that term in (1).

This set of equations was solved by the split-step Fourier method with the linear temporal part solved in the Fourier space and with the nonlinear part simulated with a fourth-order Runge–Kutta method. Diffraction was simulated with the Crank–Nicolson difference scheme in cylindrical coordinates with the absorbing boundary condition [24]. Since for solving (1–2) many computational resources are needed, we developed a GPGPU code using the OpenCL technology.

The media parameters used for the simulation are presented in Table 2. There are no data on the characteristic electron collision time in the literature, and, therefore, its value is based on the estimates for other media [7, 8]. We find values of nonlinear refractive index we used to be in agreement with model in [25]. Moreover, its dispersion is negligible for pump wavelengths we use, so we used these values unmodified.

We used the following pump radiation parameters: a Gaussian spatiotemporal profile with a 50-fs FWHM duration collimated at the medium boundary to a diameter of 120 μm (e^{-2}). The initial peak intensity was computed from the beam power as the ratio to the critical self-focusing power $P_{cr} = 3.77\pi n(\omega_0)/2k^2(\omega_0)n_2$.

It is important to note that experimental realization of SC generation should be performed very carefully to obtain reasonable results. Specifically, since nonlinear refractive index is anisotropic in halides, crystal rotation leads to change in its value which in turn leads to notable changes in generated SC. So one should either use translational motion to refresh sample [33] or use circularly polarized pump [34]. Arising depolarization in case of linear polarization can be suppressed with the appropriate choice of crystal orientation angle [33]. In the following analysis, we assume the linear polarization of the pump.

4 Results of SC simulation

To verify the results of the interference model, we performed simulation of filamentation in the media mentioned above. Later it will be shown that the simulation of filamentation in bulk media using model (1), (2) is in good agreement with the interference model. In addition, the computed SC generated during filamentation in calcium fluoride is in good agreement with the experimental data in [35]. For our simulation, we used the same parameters as in [35]; its results are shown in Fig. 3a. The correspondence is easily seen in the short-wavelength region where relatively flat spectra span from 0.7 μm up to the pump wavelength. Unfortunately, the paper [35] does not present any data for the long-wavelength region.

The results of simulation presented in Fig. 3 demonstrate the possibility of generation of a very wide SC, and its computed borders are given in Table 3. One can see from the spectra that as the central pump wavelength shifted from $\lambda_{GVD=0}$ to longer wavelengths, the wider was the SC generated, a feature that was noticed previously in various media [11, 16, 36]. However, as shown in Fig. 3b, d, moving too far leads to dips between the pump wavelength and near-IR wavelengths (which was also predicted by the interference model, see Fig. 2c, e and [20] for fused silica). With P/P_{cr}, the SC width also increases, especially in the long-wavelength region, but the main features of the spectra are retained up to $P/P_{cr} = 7$. It is important to note that such high pulse power usually does not lead to multiple filamentation [10–12, 37], so we assume that our model holds for this case. As a result, the widest SC potentially having the most stable parameters was generated in potassium iodide by a 7.5 μm pump.

Next we analyzed the SC sensitivity to those parameters of the medium that are not known very well or may significantly influence SC width (specifically, n_2, τ_c, m^* and U_i). We performed simulation for the case of potassium iodide with a 5 μm pump. These results are shown in Fig. 3e. Decrease in the nonlinear refractive index n_2 to 20×10^{-16} cm^2/W [38] led to a slight increase in the filamentation length which, in turn, slightly increased the SC generation efficiency. Increase in the characteristic electron collision time τ_c up to 10 fs (a typical value for condensed media [2]) increased the filament peak intensity. Increase in the effective electron–hole mass m^* up to 0.35 did not have a great effect on the filamentation process. Band gap decrease had large impact on filamentation process by almost doubling the filament length but SC width remained almost the same although short-wavelength boundary slightly decreased to 0.9 μm. We expected higher impact due to results presented in [39], but it seems that order of multiphoton absorption (ratio of pump photon energy to band gap, although in our simulations photoionization is not multiphoton) is already high enough for effective anti-Stokes broadening. In addition, as shown in Fig. 3f, the pump radiation parameters also do not affect the SC much. Larger beam diameter leads to longer filamentation length due to more energy in the pulse. Pulse duration increase leads to decrease in peak intensity and therefore conversion efficiency. All this again proves that in our setup the SC profile is mainly determined by dispersion of the medium and that small variations of other parameters of the medium or collimated pump radiation have a minimum impact on it.

An important point in SC generation is third harmonic generation (THG) as it may have severe impact on resulting spectra in gases [16]. It is well known that THG efficiency in bulk media is much less than one in gases due to much higher wave vector mismatch. Equation (1) does not take third harmonic generation into account, to verify

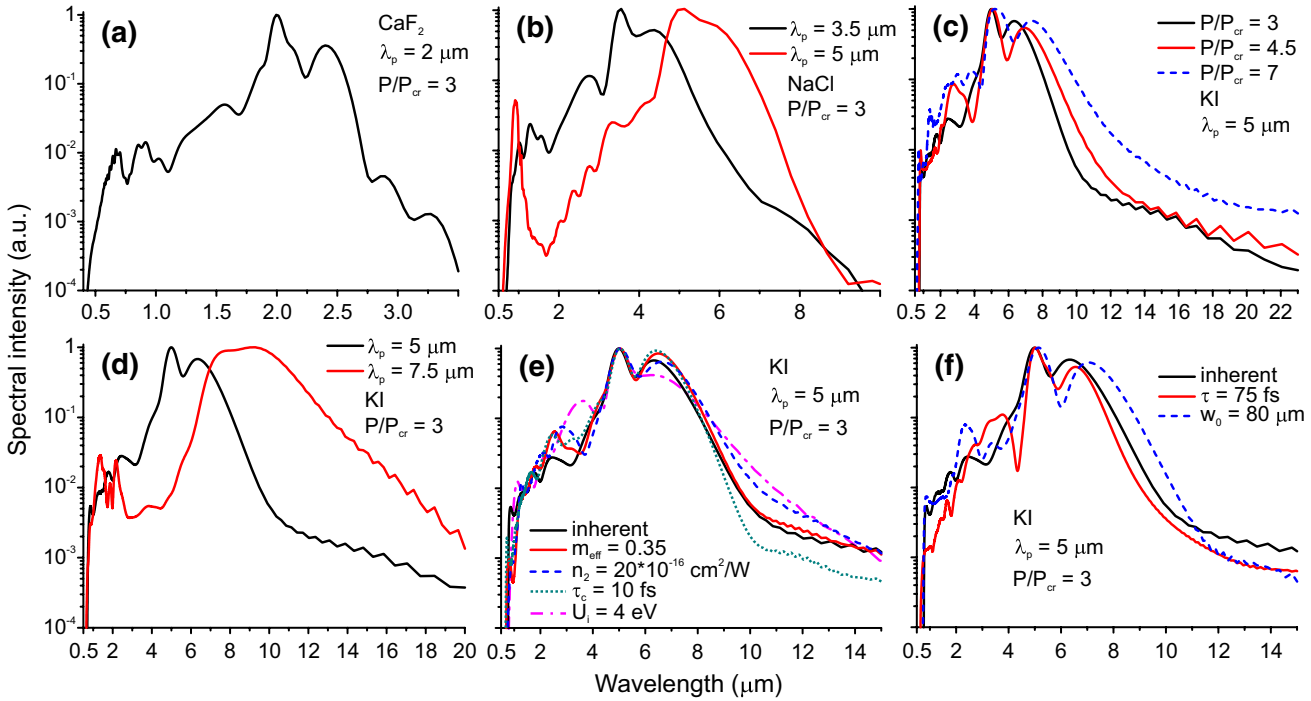

Fig. 3 SC generated in various media at exit face as simulated with equation set (1–2). **a** SC generated in calcium fluoride with 2 μm pump, $P/P_{cr} = 3$, **b** SC generated in sodium chloride with pump at different central wavelengths, $P/P_{cr} = 3$, **c** SC generated in potassium iodide with 5 μm pump with various values of P/P_{cr}, **d** SC generated in potassium iodide with pump at different central wavelengths, $P/P_{cr} = 3$, **e** SC generated in potassium iodide with 5 μm pump, $P/P_{cr} = 3$, altered medium's parameters, **f** SC generated in potassium iodide with 5 μm pump, $P/P_{cr} = 3$, altered pump radiation parameters

Table 3 SC borders at 10^{-3} level computed from the results of numerical simulation

Medium	Pump wavelength (μm)	Pump power (P_{cr})	SC range (μm)	SC width (octaves)
CaF_2	2	3	0.52–3.35	2.7
NaCl	3.5	3	0.77–7.7	3.3
NaCl	5	3	0.7–7.6	3.5
KI	5	3	0.78–16	4.4
KI	5	4.5	0.77–16	4.4
KI	5	7	0.66–22	5.1
KI	7.5	3	0.7–20.5	4.9

that THG does not influence generated SC we modified it by removing modulus at third right hand side term. Our simulations revealed that THG and other odd harmonics can be observed only at early SC buildup steps. Then it is completely "erased" with generated SC due to low THG efficiency which we conclude to be much less than 10^{-2} (a typical level of short-wavelength SC wing).

5 Peculiarities of SC evolution in an anomalous dispersion region

To better understand the processes leading to the generation of such wide spectra, let us consider the temporal dynamics of the spectra generation. Figure 4 presents a 5 μm pump pulse spectrogram evolution with propagation in potassium iodide at $P/P_{cr} = 3$. For a better view of the process in the short-wavelength region, the spectrograms are presented in frequencies. It is well known that the generation of a wide SC in this region is due to steepening of the pulse trailing edge and pulse self-compression assisted with anomalous GVD. The formation of a steep trailing edge is associated not only with Kerr nonlinearity but mostly with plasma defocusing which highly depends on order of multiphoton absorption. With this value being high in IR region, the trailing edge steepening associated with plasma defocusing is especially effective and provides SC extending up to visible range. Figure 5 shows that the

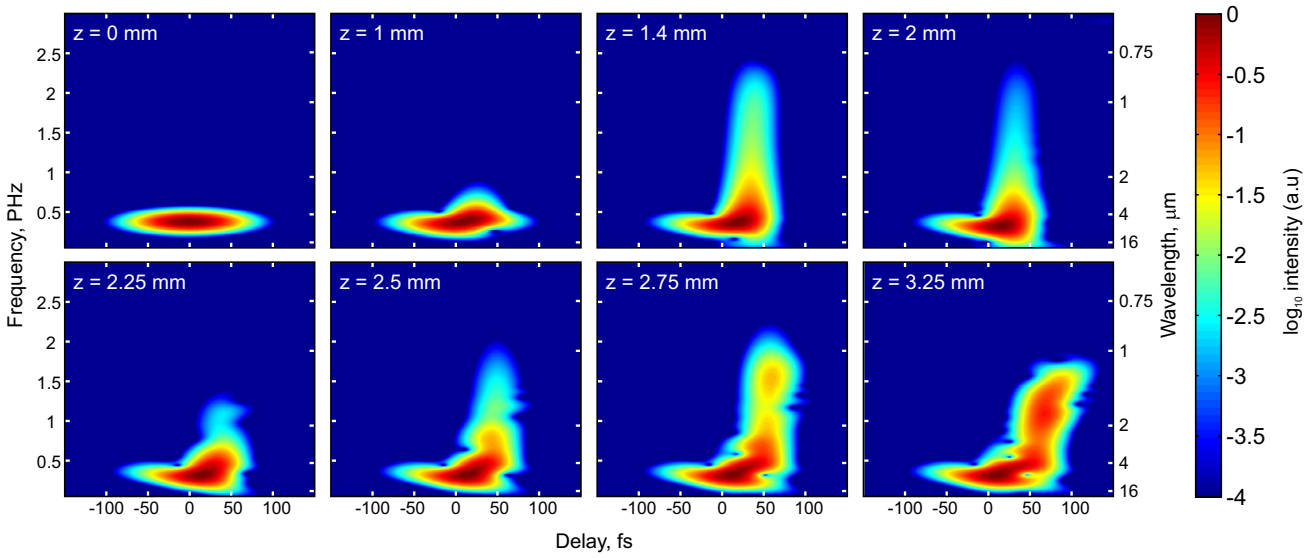

Fig. 4 On-axis pump pulse spectrograms for various propagation distances of a 5-μm pump pulse in potassium iodide, $P/P_{cr} = 3$

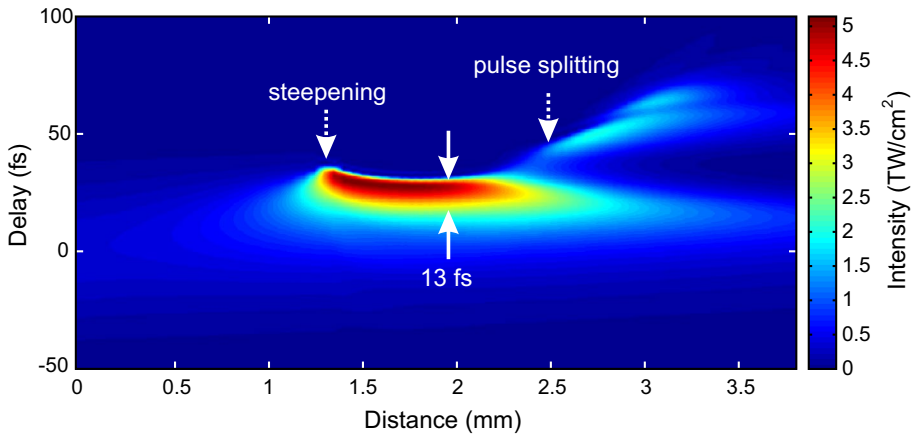

Fig. 5 On-axis temporal evolution of a 5-μm pump pulse in potassium iodide, $P/P_{cr} = 3$

steepening becomes very noticeable at $z = 1.35$ mm, where the spectrogram shows a significant spectra broadening to the short-wavelength region. Then, due to high divergence of the short-wavelength components they begin to leave the main filament in the form of a ring, the beginning of that process can be seen at $z = 2$ mm. That is why a significant growth of these components as they leave the filament is not observed at $z = 2.25$ mm where the steepening is also interrupted with pulse splitting: due to the GVD it splits into two pulses, with the trailing one having a central wavelength of 3 μm as shown in Fig. 4. Simultaneously with the split at $z = 2.5$ mm, steepening begins in the second pulse, which again causes the growth of the short-wavelength components. Low intensity and weak steepening is partly compensated by higher postpulse central frequency, although it leads to a short-wavelength SC boundary. Then the short-wavelength components continue to diverge, as can be seen in the spectrogram, up to the exit face of the medium. During filamentation, a pulse of 13 fs FWHM (35 fs e^{-2}) duration can be generated with about single period (two periods at e^{-2}) at 5-μm central wavelength.

6 Conclusions

We have analyzed some optically transparent condensed media for the possibility of generation of an ultrawideband SC in the IR region. Using the interference model, we have shown that most promising media for this are those with the highest value of $\lambda_{GVD=0}$, specifically, halides. These results have been confirmed by a numerical simulation of the filamentation process. The possibility of generation of a 4.9 octaves wide SC in potassium iodide has been demonstrated using a pump with a central wavelength of 7.5 μm.

It has been shown that variation in the parameters of the medium does not lead to a significant change in the SC. The possibility of pulse compression from 50 to 13 fs has been demonstrated.

For the first time, we have theoretically considered filamentation of far-IR radiation in halides. Their unique property, namely, a high values of $\lambda_{GVD=0}$, is connected with the possibility of generation of a very wide spectrum spanning from near to far IR, resulting in an almost 5-octave SC. Our analysis (although it was not comprehensive) has shown that no other classes of optical media except for halides have so high potential in generating near- to far-IR SC.

References

1. S. Mukamel, *Principles of Nonlinear Optical Spectroscopy* (Oxford University Press, New York, 1995)
2. A. Couairon, A. Mysyrowicz, Phys. Rep. **441**, 47 (2007)
3. P. Brumer, M. Shapiro, *Principles of the Quantum Control of Molecular Processes* (Wiley-VCH Verlag GmbH & Co., Weinheim, 2003)
4. Y. Yu, X. Gai, T. Wang, P. Ma, R. Wang, Z. Yang, B. Luther-Davies, Opt. Mater. Express **3**, 1075 (2013)
5. C.R. Petersen, U. Møller, I. Kubat, B. Zhou, S. Dupont, J. Ramsay, T. Benson, S. Sujecki, N. Abdel-Moneim, Z. Tang, D. Furniss, A. Seddon, O. Bang, Nat. Photonics **8**, 830 (2014)
6. J.K. Ranka, R.W. Schirmer, A.L. Gaeta, Phys. Rev. Lett. **77**, 3783 (1996)
7. F. Silva, D.R. Austin, A. Thai, M. Baudisch, M. Hemmer, D. Faccio, A. Couairon, J. Biegert, Nat. Commun. **3**, 807 (2012)
8. M. Durand, A. Jarnac, A. Houard, Y. Liu, S. Grabielle, N. Forget, A. Durécu, A. Couairon, A. Mysyrowicz, Phys. Rev. Lett. **110**, 115003 (2013)
9. H. Ward, L. Bergé, Phys. Rev. Lett. **90**, 053901 (2003)
10. L. Bergé, S. Skupin, Phys. Rev. E **71**, 065601 (2005)
11. S. Skupin, L. Bergé, Phys. D **220**, 14 (2006)
12. L. Bergé, S. Mauger, S. Skupin, Phys. Rev. A **81**, 013817 (2010)
13. L. Bergé, E.A. Kuznetsov, J.J. Rasmussen, Phys. Rev. E **53**, R1340 (1996)
14. L. Bergé, J.J. Rasmussen, Phys. Plasmas **3**, 824 (1996)
15. L. Bergé, Opt. Express **16**, 21529 (2008)
16. L. Bergé, J. Rolle, C. Köhler, Phys. Rev. A **88**, 023816 (2013)
17. I. Ahmad, L. Bergé, Z. Major, F. Krausz, S. Karsch, S.A. Trushin, New J. Phys. **13**, 093005 (2011)
18. D. Kartashov, S. Ališauskas, A. Pugžlys, A. Voronin, A. Zheltikov, M. Petrarca, P. Béjot, J. Kasparian, J. Wolf, A. Baltuška, Opt. Lett. **37**, 3456 (2012)
19. S.A. Frolov, V.I. Trunov, Proc. SPIE **9810**, 98100M (2015)
20. A.E. Dormidonov, V.P. Kandidov, Laser Phys. **19**, 1993 (2009)
21. A. Couairon, E. Brambilla, T. Corti, D. Majus, O.D.J. Ramírez-Góngora, M. Kolesik, Eur. Phys. J. Spec. Top. **199**, 5 (2011)
22. L.V. Keldysh, Sov. Phys. JETP **20**, 1307 (1965)
23. S. Smolorz, F. Wise, JOSA B **17**, 1636 (2000)
24. C. Vassallo, F. Collino, J. Lightwave Technol. **14**, 1570–1577 (1996)
25. M. Sheik-Bahae, D.C. Hutchings, D.J. Hagan, E.W. Van Stryland, IEEE J. Quantum Electron. **27**, 1296 (1991)
26. M. Sheik-Bahae, A.A. Said, T.H. Wei, D.J. Hagan, E.W. Van Stryland, IEEE J. Quantum Electron. **26**, 760–769 (1990)
27. R. Adair, L.L. Chase, S.A. Payne, Phys. Rev. B **39**, 3337 (1989)
28. W.L. Smith, J.H. Bechtel, N. Bloembergen, Phys. Rev. B **12**, 706 (1975)
29. M.J. Weber, *Handbook of Optical Materials* (CRC Press, New York, 2010)
30. R.S. Knox, K.J. Teegarden, in *Physics of Color' Centers*, ed. by R.S. Seymour, W.B. Fowler (Academic Press, New York, 1968)
31. I.H. Malitson, Appl. Opt. **2**, 1103 (1963)
32. H.H. Li, J. Phys. Chem. Ref. Data **5**, 329–528 (1976)
33. I. Buchvarov, A. Trifonov, T. Fiebig, Opt. Lett. **32**, 1539 (2007)
34. P. Johnson, V.I. Prokhorenko, R.J. Miller, Opt. Express **17**, 21488 (2009)
35. J. Darginavičius, D. Majus, V. Jukna, N. Garejev, G. Valiulis, A. Couairon, A. Dubietis, Opt. Express **21**, 25210 (2013)
36. S. Skupin, L. Bergé, Opt. Commun. **280**, 173 (2007)
37. G. Fibich, *Self-Focusing: Past and Present* (Springer, New York, 2009)
38. A. Penzkofer, J. Schmailzi, H. Glas, Appl. Phys. B **29**, 37 (1982)
39. C. Nagura, A. Suda, H. Kawano, M. Obara, K. Midorikawa, Appl. Opt. **41**, 3735 (2002)